Chem Soc Rev

Water-soluble Perylenediimides: Design Concepts and Biological Applications

Journal:	*Chemical Society Reviews*
Manuscript ID	CS-SYN-10-2015-000754.R2
Article Type:	Tutorial Review
Date Submitted by the Author:	02-Jan-2016
Complete List of Authors:	Yin, Meizhen; Beijing University of Chemical Technology, ; Max Planck Institute for Polymer Research, Sun, Mengmeng; Beijing University of Chemical Technology Beijing, Muellen, K; Max-Planck-Institut fur Polymerforschung, Max-Planck-Institut fur Polymerforschung

Journal Name

ARTICLE

Water-soluble Perylenediimides: Design Concepts and Biological Applications

Received 00th January 20xx,

Accepted 00th January 20xx

DOI: 10.1039/x0xx00000x

www.rsc.org/

Mengmeng Sun,[a] Klaus Müllen[b] and Meizhen Yin*[a]

Water-soluble perylenediimides (PDIs) with high fluorescence intensity, photostability and biocompatibility have been successfully prepared and applied in biological field. In this tutorial review, we briefly focus on the synthetic strategies toward water-soluble PDIs by incorporating ionic or non-ionic substituents with multiple polar groups into the *bay*-region, *imide*- or *ortho*-positions of PDIs. These ionic/non-ionic substituents can suppress the π-π aggregation and shield the inner perylene chromophores, thus contribute to the water solubility which is essential for biological application. The optical properties, absorption and emission maxima above 500 nm, minimize the autofluorescence background of cells and provide the access to image in living cells. The biological applications of water-soluble PDIs are discussed from simple (basic) to complex (advanced) processes, including biosensing *in vitro* studies, imaging and gene/drug delivering in living cells, tissues and the whole body. The promising future of designed multi-functional water-soluble PDIs will be highlighted in this review.

Key learning points

(1) The chemical structure affects the physical and optical characteristics

(2) Hydrophilic substituents (cationic, anionic or non-ionic polar groups) improve the water solubility

(3) Fluorescence-based techniques for biosensing and bioimaging

(4) Nanocarrier for gene/drug delivery

(5) *in vitro* and *in vivo* assays (living cells, tissues and the whole body)

1. Introduction

Fluorescence-based techniques have been widely applied in the visualization of biological components and processes due to their high selectivity and sensitivity. A successful fluorophores for biosensing or bioimaging should possess some unique properties, such as high water-solubility, fluorescence intensity, photostability and biocompatibility. As an attractive class of chromophores, perylene-3,4,9,10-tetracarboxylic acid diimides (perylene diimides, PDIs) have been widely used as active components of field-effect transistors (OFET)[1] and organic light-emitting diodes (OLED),[2] and as dye sensitizers in solar cells[3, 4] because of their high extinction coefficients, high fluorescence quantum yields (FQYs), broad color range, as well as outstanding chemical, thermal, and photochemical stability in organic solvents. Especially, the absorption and emission maxima of PDIs are above 500 nm, which minimize the autofluorescence background of living cells. However, PDIs exhibit poor water solubility, very weak fluorescence in aqueous solution, and the tendency to form aggregates due to the intrinsic π-π stacking interactions between perylene backbones.[5, 6] This creates a major challenge for the application of PDIs in the biological and medicinal fields. Great efforts have been made to increase the water solubility of PDIs by introducing hydrophilic groups in the *bay*-region or at the *imide*- and *ortho*-positions.

Ionic groups such as cationic ammonium salts,[7-9] anionic carboxylic acids,[10] sulfonic acids[11] and phosphonic acids[12] have been directly incorporated into perylene chromophores to generate water-soluble PDIs. Another powerful strategy to enhance water solubility is the attachment of non-ionic substituents with multiple polar groups, such as poly(ethylene glycol) (PEG), polyglycerol (PG) dendrons, and dendritic carbohydrate derivatives, in the bay region or at the imide positions of PDI. These approaches effectively obstruct aggregation of the perylene cores, and the functionalized PDIs exhibit strong fluorescence and high FQYs in aqueous solution.

In this tutorial review, we briefly present the synthetic strategies toward water-soluble PDIs by incorporating ionic or non-ionic substituents with multiple polar groups into the *bay*-region, *imide*- or *ortho*-positions of PDIs. These ionic/non-ionic substituents can suppress the π-π stacking of the inner perylene chromophores, and also contribute to the biocompatibility. The optical properties and biological applications of water-soluble PDIs are discussed with a special

[a] *State Key Laboratory of Chemical Resource Engineering, Key Laboratory of Carbon Fiber and Functional Polymers of Ministry of Education, Beijing Laboratory of Biomedical Materials, Beijing University of Chemical Technology, 100029, Beijing, China. E-mail: yinmz@mail.buct.edu.cn*

[b] *Max-Planck Institut für Polymerforschung, Ackermannweg 10, 55128, Mainz, Germany.*

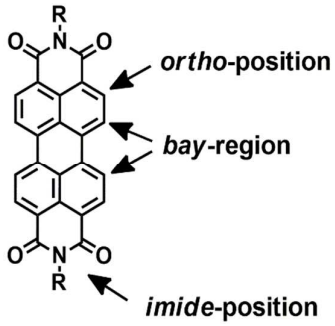

Fig. 1 General structure of PDIs.

focus on their biosensing and bioimaging applications in living cells, tissues, and the whole body. Moreover, benefiting from the positive charges or cavities provided by dendrimers, PDIs can be used as nanocarriers for gene/drug delivery and achieve gene therapy or chemotherapy.

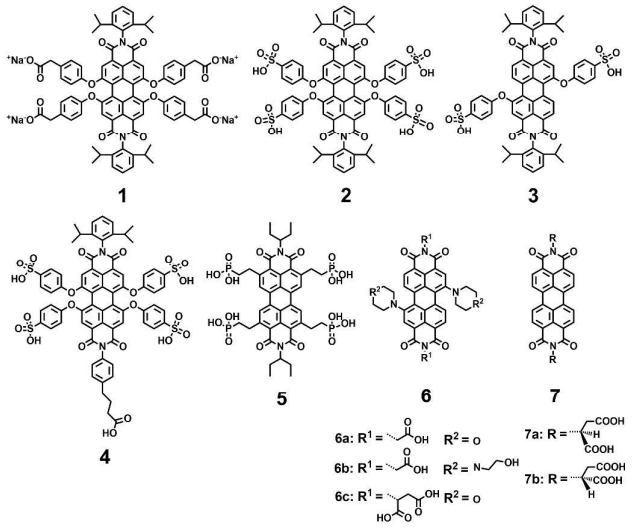

Fig. 2 PDIs **1**-**7** with small negatively charged substituents.

2. Design of water-soluble perylenediimide chromophores

In general, PDIs are chemically modified in the *bay*-region, *imide*- or *ortho*-positions of PDIs (Fig. 1). The substituents at the *imide*-positions are primarily used to tune the solubility of PDIs in various solvents while minimally altering the optical and electronic properties. The resulting derivatives retain the green-yellow emission of PDIs and their high FQYs. In contrast, modifications in the *bay*-region of PDIs result in a twist of the two naphthalene rings, which can tune the spectroscopic properties and yield a significant red shift in the absorption maximum with an increased Stokes shift. This has attracted great interests in biological and medicinal research because it can minimize phototoxicity and interference from biological auto-fluorescence. Selective functionalization in the *ortho*-positions can successfully tune the optical and electronic properties without affecting the planarity of the perylene core. Moreover, the solid state emission and solubility in organic solvents are significantly enhanced compared to the unsubstituted PDIs.[13-16] Typically, ionic or non-ionic functions with multiple polar groups such as -SO_3H, -OH, -NH_2, -NHR, -COOH, -O- are introduced into modified PDIs to enhance the water-solubility, because these groups can form hydrogen bonds between the polar pendant groups and water molecules. In addition, the polar substituents attenuate intermolecular π-π aggregation of PDIs due to the steric hindrance or electrostatic repulsion forces.[9]

2.1 Anionic Substituents

Anionic substituents, such as carboxylic, sulfonic and phosphonic acids and their corresponding salts, are the most widely used to improve the water-solubility of PDIs. Müllen and coworkers[9, 12, 17] reported a series of water-soluble PDIs with anionic substituents in the *bay*-region. Compound **1**, containing four carboxylic acid sodium salts attached at the *bay*-region, was prepared by reacting the parent acid with sodium hydroxide. The carboxylates improve the water solubility, while the chromophore with four carboxylic acid substituents is not soluble in water. Compound **2**, containing four sulfonic acids at the *bay*-region, had a water solubility of 8.0×10^{-2} mol/L. With decreasing number of hydrophilic groups-from four down to two, the water solubility and fluorescence quantum yield (FQY) of **3** decreased (FQY=12%). The monofunctional PDI **4** showed similar water solubility as the symmetric ionic PDIs **2**. In addition, **4** can be further functionalized due to the presence of a carboxylic acid handle at the *imide*-positions of PDI. The fluorescence quantum yield (FQY) of **2** is 58%, displaying a reduction of 42% compared to PDI chromophores in organic solvents (FQY≈100%). The reduction of the FQY in polar solvents was explained by the aggregation, vibrational relaxation and photoinduced electron-transfer (PET). Compound **1** bearing carboxylate groups at the terminus of a short alkyl spacer displays a low FQY of 7%, due to the lipophilic and vibrational relaxation resulting from the alkyl spacers. The FQY of **4** is slightly lower (49%) than that of **2**, because the imide substitution affects the fluorescence of PDIs in water. Compound **5** with phosphonic acids in *ortho*-positions is capable of carrying negative charges at biologically relevant pH values, with enhanced resistance to aggregation and fluorescence quenching. The FQY of **5** is 77% in water. Because of the water-solubility and high FQY, **5** was impregnated into HeLa cells for successful labeling. Akkaya and coworkers synthesized several water-soluble green PDI dyes (**6a-c**) by introducing dialkylamino groups onto the *bay*-region.[18] Under red light excitation, **6c** was shown to be efficient generators of singlet oxygen and displayed significant light-induced cytotoxic effects on the living cells. A pair of chiral PDIs (**7a**-**b**) with aspartic acid (L or D) at the *imide*-positions was prepared by Malik and coworkers.[19] After the pH was decreased to 4.00, these two enantiomers formed reddish-brown hydrogel with reddish color under UV light. Dried **7a** or **7b** gel formed well-defined left- or right-handed helical fibers of 20 nm diameter with an average pitch length

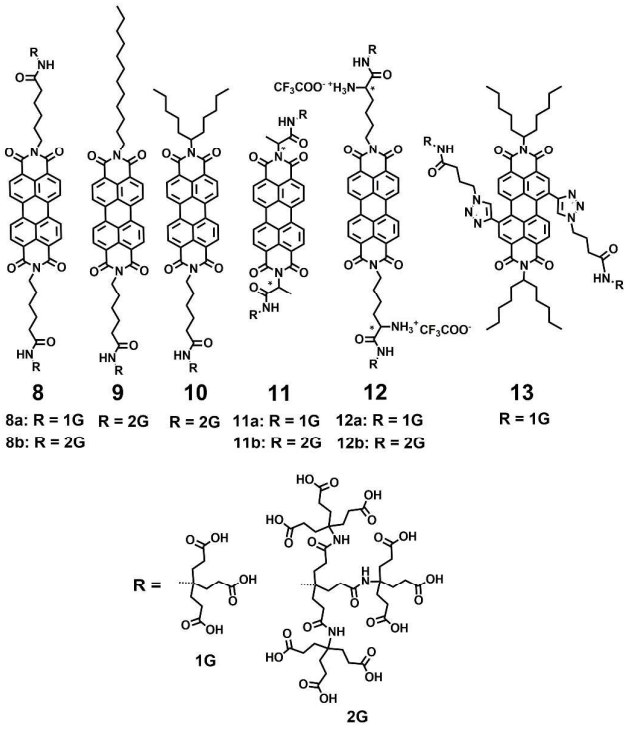

Fig. 3 PDIs **8**-**13** with Newkome-type carboxylates.

of 20 nm. The perylene core forced **7a** or **7b** to coil until thick filaments were formed. These fibers maintained the original helical of the subunit and were stabilized by π-π stacking of the perylene core and hydrogen bonding interactions of the carboxyl groups.

Newkome and coworkers described the synthesis of 1→3 C-branched polyamide dendrons (named Newkome-type dendrons) firstly.[20] The terminal carboxylic acids were easily hydrolyzed starting from peripheral esters, and consequently enhanced solubility of hydrophobic groups in aqueous media. Moreover, the peripheral carboxylic acids served as active sites for growing dendrons or coupling with biologically active species in medical applications. Hirsch and coworkers[21-23] synthesized a series of water-soluble symmetric and asymmetric, chiral and achiral PDIs by incorporating first-generation (1G) and second-generation (2G) Newkome-type dendrons at the *imide*-positions (**8**-**12**) or in the *bay*-region (**13**). The polyamide dendrons act as hydrophilic substituents to enhance water solubility and also exert an aggregation-inhibiting effect because of their bulkiness and anionic character, which can be easily generated in a buffer solution at pH 7.2. The symmetric 1G dendronized dye **8a** forms aggregates more easily than its 2G-counterpart **8b**. The perylene core in **8b** is effectively shielded due to the increased steric demand of the dendron units and electrostatic repulsion, as most of the 18 carboxy groups are deprotonated at neutral pH. The asymmetric derivative **9** reveals pronounced aggregation properties due to the presence of both a 2G-dendron and a flexible and non-bulky dodecyl substituent, and forms regularly shaped micelles in water (pH = 7.2) with a

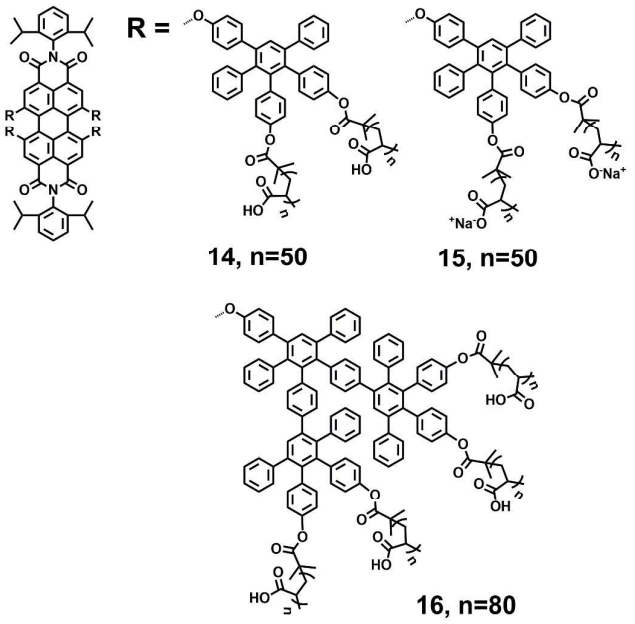

Fig. 4 PDIs **14**-**16** with polymeric carboxylates.

mean diameter of 16 nm. However, its 1G-analogue is not soluble in water, because the presence of just one 1G-dendron does not provide sufficient overall hydrophilicity. Asymmetric PDIs **10** with 2G-dendron is water soluble; however, its 1G-counterpart, bearing only three acid groups, is insoluble in water. The symmetric and chiral PDIs **11** and **12** are connected with 1G or 2G Newkome-type dendrimers by the amino acids alanine and lysine, respectively. The formation of chiral superstructures of **11a** was found to be pH- and concentration-dependent. Compound **13** is amphiphilic PDIs with 1G-dendron in the *bay*-regions. The symmetric 1G-dendronized dyes **8a**, **11a** and **12a** form aggregates more easily than its 2G-counterparts **8b**, **11b** and **12b**, due to the bulkiness of dendritic carboxylates.

Müllen and coworkers described a method for the rapid construction of branched polyphenylene dendrimers by Diels-Alder cycloaddition in 1997.[24] Three-dimensional polyphenylene dendrimers are shape-persistent and out-of-plane twisted phenyl components. Yin et al[25-27] reported types of negatively charged fluorescent core–shell macromolecules (**14, 15** and **16**) consisting of a central PDI chromophore, surrounded by hydrophobic polyphenylene dendrimers and outer flexible polymers. Compared with the above polyamide dendrons, the polyphenylene dendrimers are bulkier and more rigid, which can more effectively suppress aggregation and shield the inner perylene chromophores. The outer polymer shells with multiple carboxylic acids, introduced by atom transfer radical polymerization (ATRP), contribute to the water solubility and charge densities of the core–shell macromolecules. PDIs **14** and **15** are the 1G polyphenylene dendrimer, bearing eight arms with multiple carboxylic acids and corresponding sodium salts. **16** is the 2G analogue, bearing sixteen arms with multiple carboxylic acids. PDIs **14**, **15** and **16** exhibit water solubilities of > 10 g/L in aqueous media.

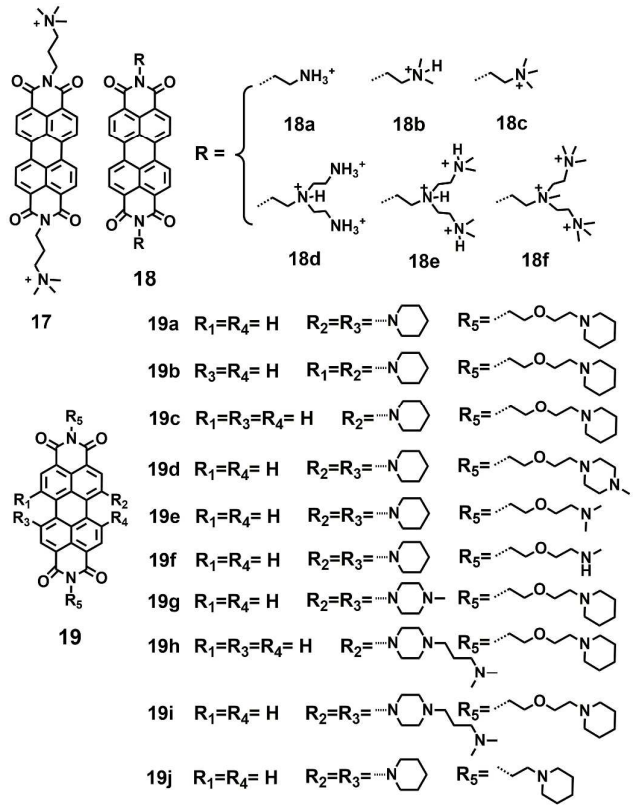

Fig. 5 Imide or bay substituted-PDIs **17**, **18** (**a**-**f**) and **19** (**a**-**j**) with primary, secondary, tertiary or quaternized ammonium salts and tertiary amines.

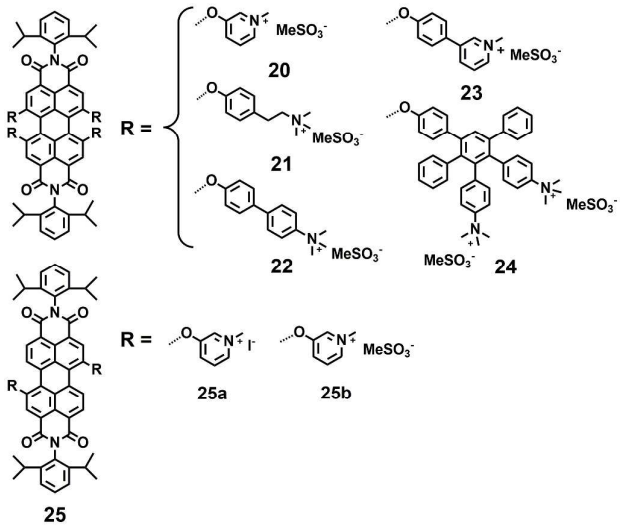

Fig. 6 Bay substituted-PDIs **20**-**25** with quaternized ammonium salts

The FQYs of **14** and **16** are 13% and 22% in water, respectively. PDI **14** (n=55) forms unimolecular fluorescent polymeric micelles (UFPM) in aqueous solution.[28] The size and the fluorescence intensity of the UFPM are pH-sensitive due to the polyelectrolytic nature of the outer polymer shell.

2.2 Cationic substituents

Hydrophobic dyes can be generally converted into water-soluble dyes by adding positively charged substituents. Nitrogen-containing functional groups often carry positive charges, and for this reason, cationic protonated amines (primary, secondary, tertiary and quaternary ammonium salts) are widely used to improve the water-solubility of PDIs.

A cationic PDI **17** with two positive charges was reported as a fluorescent probe by Yu.[29] Its considerable water solubility (>30 mM) was provided by the two positive charges. Due to the repulsive interactions between the electrostatic charges, the tendency of PDI to aggregate decreased. Thus, **17** existed in both aggregated form and free monomeric form in aqueous solution. Yin and coworkers[30] reported a series of water-soluble symmetric cationic PDIs **18** (**a**-**f**), which inhibit cancer cell growth as DNA intercalators. These PDIs contain a fluorescent perylene core and various protonated amines at the imide positions. Their nano-size and planar structure allow intercalation into double-stranded DNA base pairs. The water solubility is greatly increased due to the positive charges afforded by these protonated amines. PDIs **18c** and **18f** containing quaternary ammonium cations show higher water solubility (>10 g/L in water) than that of **18a** and **18d** carrying primary ammonium salts (≤ 2 g/L in water). The FQYs of **18** (**a**-**f**) are 1.1%, 22.8%, 26.2%, 4.7%, 5.6% and 25.3%, respectively. PDI **18b** exhibits low cytotoxicity with a cell viability of 90% to non-cancer cells. PDIs **18b**, **18c**, and **18e** can specifically accumulate in the cell nuclei of animal tissues by intercalation and electrostatic interaction with DNA. A series of PDIs **19** with different *N*-cyclic substituents in the *bay*-region and different side chains at the *imide*-position is reported by Franceschin and coworkers.[31] Their respective water-soluble hydrochlorides were prepared by precipitation with diethyl ether from an acidic (HCl) solution of methanol.

Müllen and coworkers[9, 17] also reported a series of water-soluble positively charged PDIs (**20**-**25**) by quaternization of dimethylamino or pyridinium-substitutes in the *bay*-regions of PDI. Chromophore **20** possesses the highest solubility in water (8.0×10^{-2} mol/L), while **25** with two hydrophilic groups exhibits low water solubility. The hydrophilic groups directly located on the phenyl ring (**20**) lead to a high FQY (66%), while those located at the terminus of a short alkyl chain (**21**) lead to a low FQY of 14%. The introduction of additional phenylene rings (**22** and **23**) produces highly lipophilic compounds with very limited water solubility and results in low FQYs in water (11%, 23%). The bulky and rigid dendritic polyphenylene dendrimer branches can effectively suppress aggregation and shield the inner chromophores. However, polyphenylene dendrimer **24** displays only weak FQY (15%), which is mainly attributed to energy loss through vibrational relaxation.[32] PDI **25b** with two positively charged pyridinium substituents exhibits sufficient water solubility and high FQY (98%), due to the suppressing PET processes by a minimum number of functional groups.

Montalti and coworkers synthesized a fluorescent polyetheramine **26** by microwave assisted reaction.[33] PDI **26** can disperse in water and self-assemble into non-fluorescent nanoparticles. Hirsch and coworkers[34] synthesized a series of

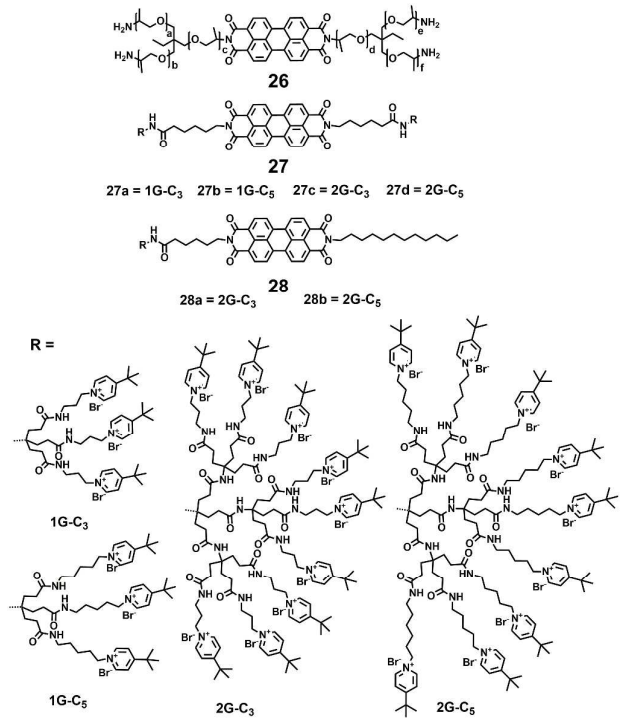

Fig. 7 Fluorescent polyetheramine **26** and PDI-cored cationic pyridinium dendrimers **27**-**28**.

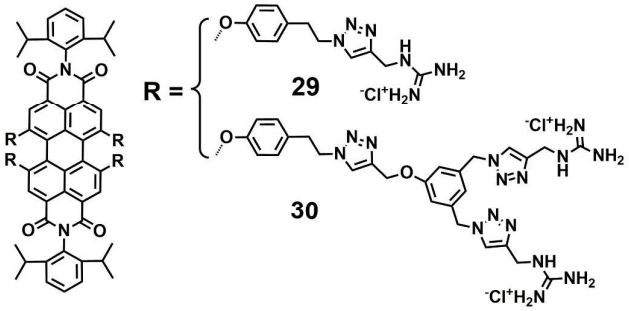

Fig. 8 Guanidinium-dendronized PDIs **29**-**30.**

symmetric and asymmetric dendronized polycationic PDIs, **27** and **28**, by using amide coupling reactions of pyridinium salt head groups with terminal carboxylic groups of PDIs **8** and **9**. The water solubility of **27** and **28** is provided by the positively charged pyridinium salts at the periphery of these PDIs and are independent of the pH. Compared with **27a** and **27b** containing small 1G dendrons, all the 2G dendronized PDIs (**27c**, **27d**, **28a** and **28b)** exhibit a pronounced increase in water-solubility, owing to the steric hindrance of larger dendrons in the perylene stacking and aggregation. The FQYs of **27c**, **27d**, **28a** and **28b** are 63%, 79%, 68% and 69% in water, respectively. In contrast, the fluorescence of **27a** and **27b** is clearly quenched in water with low FQYs (7% and 0.11%). This observation is explained by a radiation free decay from the excited state due to the close proximity of aggregated molecules.[34]

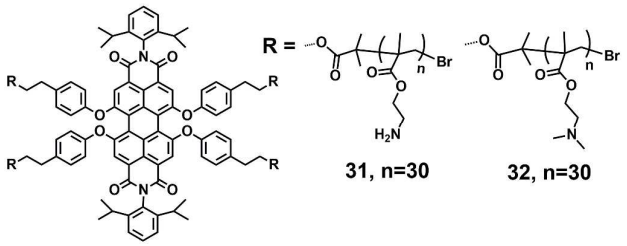

Fig. 9 PDI-cored star polycations **31**-**32.**

A class of highly photostable and water-soluble guanidinium-dendronized PDIs were synthesized by utilizing the copper-catalyzed azide–alkyne cycloaddition (''click'') reaction.[35] These dendronized guanidinium moieties were introduced to suppress the aggregation of the central PDI chromophore in water. Also the electrostatic repulsions of positive guanidinium moieties will further minimize the aggregation. Due to the planar conformation and high basicity of guanidine (pKa=13.5), the guanidinium moieties can form strong ion pairs with oxoanions, ensuring protonation and positively charged over a wide pH range. PDI **29**, bearing four guanidinium end groups, only dissolved in hot water and exhibited nearly no fluorescence. In contrast, **30**, containing eight analogues, showed increased water solubility with a FQY of 39%. Such differences are ascribed mainly to the lower number of guanidinium moieties, which cannot provide sufficient inhibition of aggregation and overall hydrophilicity. The moderate FQY for **30** is mainly due to substituents at the *bay*-regions of PDIs, which decreases the planarity of the aromatic scaffold. The cell viability of **30** treated cells was higher than 90% at concentrations of 5 mM, indicating low toxicity of **30**.

Two water-soluble PDI-cored star polycations, **31** and **32**, with two different amines in the bay region of PDI, were synthesized by ATRP.[36] The star polycations consist of a fluorescent central PDI and outer polymer arms of poly(2-aminoethyl methacrylate)(PAEMA, **31**) or poly(2-(dimethylamino)ethyl methacrylate) (PDMAEMA, **32**). PAEMA or PDMAEMA provides water solubility, due to the presence of polar groups such as $–NH_2$, –OCO– and $–N(R)_2$, which can form hydrogen bonds with water molecules. Linear concentration-dependent absorptions of **31** and **32** are observed in aqueous solutions, suggesting that both **31** and **32** stay in a single-molecule state over the whole concentration range studied (7.26-28.9 μM). In addition, the maximum emission peaks is located at 622 nm, thus **31** and **32** with good FQYs (14% and 6%) are well-suited for single-molecule fluorescence detection and fluorescence tracing and imaging in live cell experiments. The high zeta potentials of **31** and **32** (37.8 and 56.5) provide the possibility to complex with DNA via electrostatic interactions.

Yin et al[25, 27, 37] synthesized several water soluble fluorescent core–shell macromolecules (**33**-**36**) surrounded by polyphenylenes dendrimer grafting with positive charged polymer chains. The architectures consist of a fluorescent central PDI surrounded by 1G and 2G polyphenylene

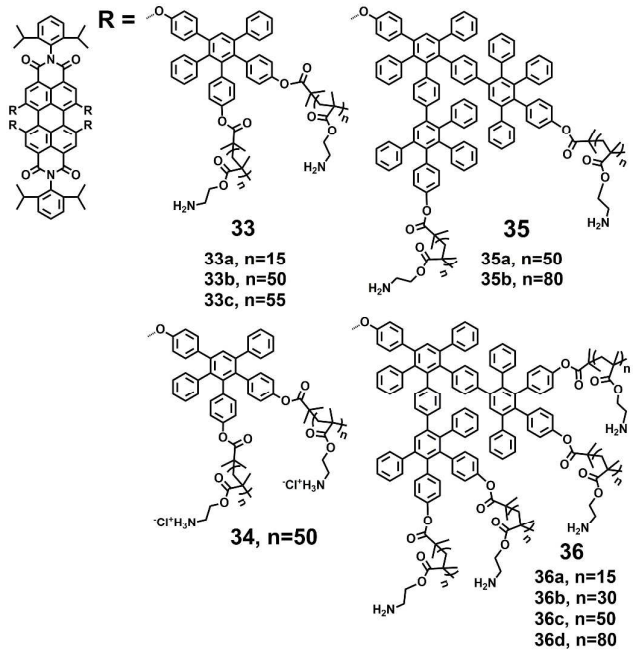

Fig. 10 PDIs **33**-**36** with polymeric amines.

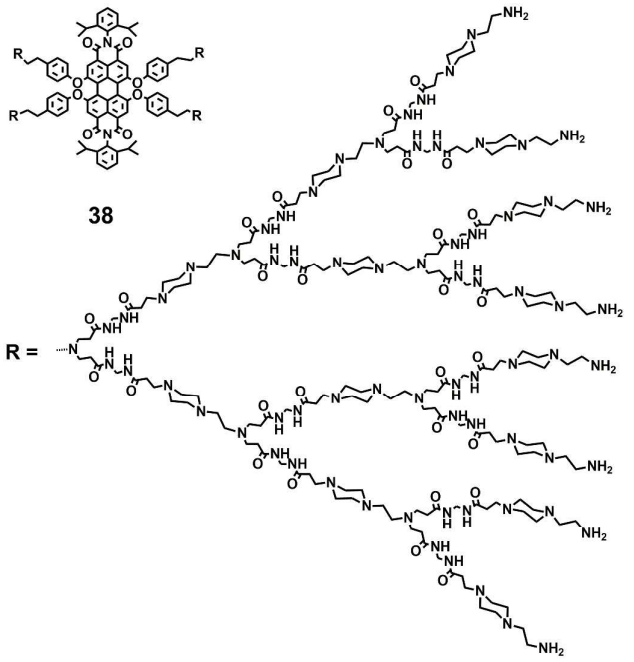

Fig. 12. PDI-cored cationic PDI-PAmAm dendrimer **37**.

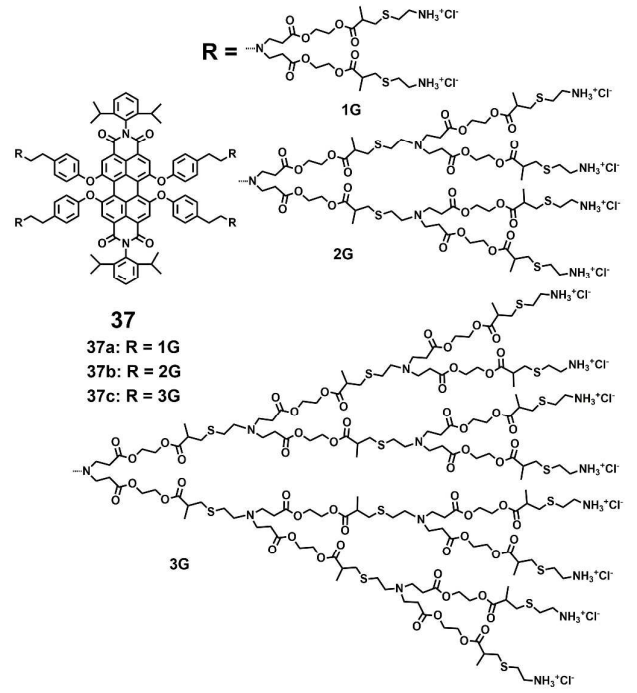

Fig. 11 PDI-cored cationic dendrimers **37** (**a**-**c**).

dendrimers and an outer polymer shell with multiple amine groups. The rigid polyphenylene dendrimer shell prevents the PDI chromophore from aggregation in water, and the outer polymer shell with multiple amine groups provides water solubility (> 10 g/L) with FQYs varying from 7.6% to 16.8%. The absorption maxima exhibits bathochromic shifts for those macromolecules with a higher number of amino groups (**36b**, **36c**, **36d**). This trend is also observed in emission spectra: emission intensities increase and emission maxima shift bathochromically with increasing numbers of repeating units.

A series of water-soluble PDI-cored cationic dendrimers, **37**(**a**-**c**), with three generations synthesized via a "click" reaction were reported by Yin and coworkers.[38] The central fluorescent PDI chromophore allows the tracing of cell uptake via fluorescence microscopy. The peripheral primary amines provide positive charges upon a final treatment with hydrochloric acid. The outer cationic dendrimers noticeably suppress the aggregation of the encapsulated PDI chromophores due to the steric hindrance and electrostatic repulsion forces. The peripheral primary amines and multiple polar groups (–OCO– and –S–) enhance the water solubility. All the dendrimers show a water solubility of above 10 g/L and high photostability. The absorbance, fluorescence intensities and FQYs of **37**(**a**-**c**) (9%, 12% and 25%) in water increase with higher dendron generation. The cell viabilities of **37**(**a**-**c**) were all above 90% at concentrations of 6 mM, showing that the dendrimers exhibit low cytotoxicity.

Apart from the advantages in water solubility and photostability, **37**(**a**-**c**) have some shortcomings such as the instability of the outer dendritic polyester units under basic conditions, which have to be treated with diluted hydrochloric acid to yield their ammonium salts. Subsequently, Yin and coworkers[39] developed the water soluble PDI-cored cationic dendrimer **38** by incorporating the poly(amido amine) (PAmAm) dendritic units into the *bay*-regions of PDIs. The increased water solubility (>20 g/L) and chemical stability are resulting from the more polar and stable building blocks –CONH– in the PAmAm dendritic units, together with the polar groups $–N(R)_2$. The linear concentration-dependent

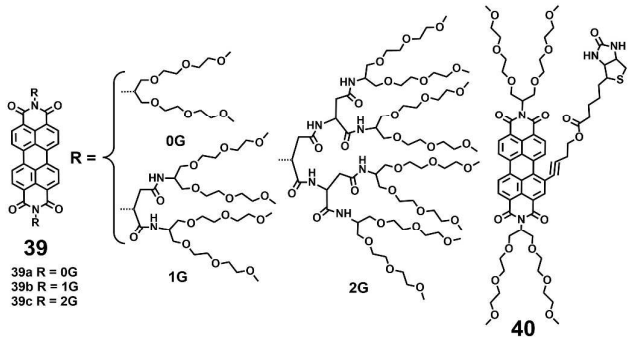

Fig. 13 PDI-cored PEG dendrimer **39** (**a**-**c**) and **40** with attached biotin ligand.

absorbance implies that **38** exists in a typically monomeric form in the concentration range of 0.2 μM to 2.0 μM. The PAmAm shell provides the steric bulkiness with electrostatic repulsion forces that notably suppresses aggregation of the central PDI chromophore in aqueous solution. The FQY of **38** is 18% in water. The cell viabilities of **38** treated cells are higher than 92% at all the concentrations studied (1-4 μM), indicating that **38** has low cell toxicity.

2.3 Non-ionic substituents

Compared with the ionic hydrophilic groups, the non-ionic hydrophilic groups possess the unique advantages of pH and ionic strength insensitivities in biological buffer systems. The non-ionic hydrophilic groups also minimizes undesired nonspecific ionic interactions that may occur with membranes and other charged biomolecules. Widely used non-ionic substituents, which were introduced to improve the water-solubility of PDIs, are poly(ethylene glycol) (PEG), polyglycerol (PG) dendrons, and dendritic carbohydrate derivatives. These non-ionic bulky substituents provide an effective steric hindrance that weakens the π–π interactions between the PDI backbones. Furthermore, the non-ionic substituents consist of multiple polar groups such as ether and hydroxyl, which can form hydrogen bonds with water molecules and lead to water solubility.

A series of PDI-cored PEG dendrimers **39**(**a**-**c**) were synthesized.[40] These PDIs consist of a PDI fluorescent core, branched oligo(glutamic acid)s, and PEG chains. The branched oligo (glutamic acid)s function as scaffolds to suppress the aggregation of the central PDI. Dye **39a** bearing 0G dendrons exists in an aggregated state over the whole accessible concentration range (1×10^{-6}-1×10^{-4} M) evidenced by a broad absorption spectrum with a hypochromically shifted absorption maximum and a weak fluorescence (4%). With higher dendron generation (**39b** and **39c)**, the steric hindrance increases, leading to improved hydrophilicity of PDIs. Moreover, the FQYs of **39b** and **39c** also increase in water (65% and 93%), because the PDI fluorophores are efficient emitters in water as their aggregation is completely suppressed. PDIs **39**(**a**-**c**) show very low cytotoxicity (over 90% cell viability) using 3-(4,5-dimethylthiazol-2-yl)-2,5-diphenyl tetrazolium bromide (MTT) cell-viability assay, because PEG chains prevent the dyes from interacting nonspecifically with

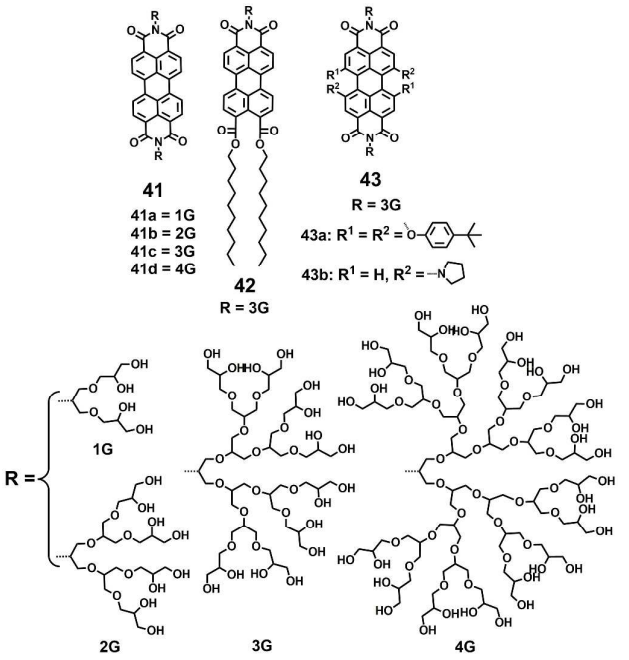

Fig. 14 PDI-cored PG dendrimers **41-43**.

the extracellular proteins. In further studies, the authors prepared a *bay* substituted PDI **40** with a biotin ligand.[41] Compound **40** can form self-assembled nanostructures with high stability in aqueous solution, leading to complete quenching of fluorescence.

Haag and coworkers[42-44] synthesized a series of neutral, water-soluble PG-dendronized PDIs with high FQYs. The 1G dendronized PDI **41a** exhibits the typical absorption spectra of the aggregated form over the whole accessible concentration range (1×10^{-6}-1×10^{-4} M), as the 1G dendron at the imide position is apparently too small to shield the perylene core and suppress the aggregation. With increased PG dendron generation, aggregation is inhibited. The observed absorption spectra of **41c** and **41d** bearing 3G and 4G dendrons arise from PDI monomers over the whole concentration range because these dendrons are sufficiently large to shield the π surfaces of the PDI. The FQYs of **41**(**a**-**d**) also reveal a continuous increase from 33% for 1G substituted **41a** up to 99% for 4G substituted **41d** with increasing dendron generation, due to the strong dendritic effect. Optical studies and dynamic light scattering reveal that **42** forms spherical micelles with a narrow size distribution and very low FQY (1%) in water, due to the aggregation of PDI core. MTT assay show that **42** is completely nontoxic to cells even at the concentrations of 10^{-5} M. Upon gradually increasing the temperature from 298 K to 368 K, **43a** displays a transition from an aggregated state into monomeric species, as proven by the typical characteristics in temperature- dependent fluorescence measurements and ^{1}H NMR spectroscopy. Notably, the FQY of **43a** is still low (1.1%) even at high temperatures. The quenched fluorescence can be explained by PET mechanism from the phenoxy groups to the PDI core. The 3G-dendronized **43b** maintains monomeric

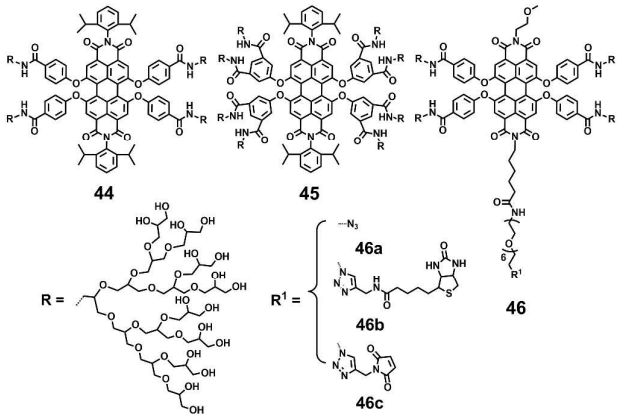

Fig. 15 PDI-cored PG dendrimers **44-46.**

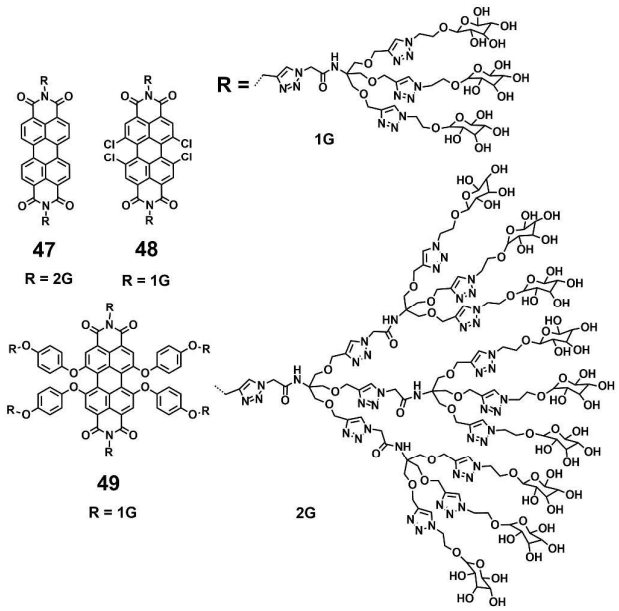

Fig. 16 PDI-cored glycodendrimer **47**-**49**.

species over the whole accessible concentration, but is almost nonfluorescent in water (FQY=0.2%). The low FQY is again related to PET from the electron-rich pyrrolidine to the electron-poor PDI.

Introduction of functional groups in the *bay*-region of PDIs results in a significant red shift of the absorption maximum and an increased Stokes shift, minimizing phototoxicity and interference from biological auto-fluorescence. Zimmerman and coworkers[39] developed several neutral water-soluble PDIs (**44**, **45** and **46**) that are *bay*-substituted by amide coupling of the PDI cores with amine-functionalized PG dendrons.[45] The PG dendrons provide the steric bulkiness necessary to minimize π–π interactions of the perylene cores. Compounds **46b** and **46c** were obtained by the click reactions of monofunctional **46a** with alkyne-functionalized biotin and maleimide. All these neutral PDIs are water-soluble and highly fluorescent in water with FQYs ranging from 57% to 83%. The difference can be attributed to the varying degrees of encapsulation and solubilization of PDIs within the PG dendritic shell. The bulkier and more substituted **45** exhibits the highest FQY of 83%, due to the more effective encapsulation and solubilization of the PDI core by eight dendrons carrying a total of 128 peripheral hydroxyl groups. In further studies, intramolecular crosslinking of the dendronized and hyperbranched PG, which is substituted at *bay*-region of PDI, were reported.[46, 47] The crosslinking results in a significant reduction in the FQY, due to the decrease of hydroxyl end-groups causing lower aqueous solubility.

Water soluble PDIs (**47**-**49**) modified by glycodendrimers at the *imide*-positions or *bay*-region have been synthesized through the click reaction and subsequent removal of protecting groups.[48-50] Upon gradual increase of the concentration and decrease of temperature, the UV–vis spectra of **47** and **48** display the typical spectral characteristics of monomeric to aggregated state, indicating that the π-π aggregation of these PDIs is concentration- and temperature-dependent. The concentration-dependent aggregation of **46** and **48** also affects the FQYs: at low concentration of 5.0×10^{-6} M, the FQYs of **47** and **48** are 59.9% and 54%, respectively. With increasing concentration, the fluorescence emission is gradually quenched, accompanied by a bathochromic shift because of the aggregation. Notable, **49** bearing glycodendrimers both at the *imide*-positions and *bay*-regions was barely detectable by fluorescence because of intramolecular electronic transfer process from the electron-rich substituents (triazole group) to the PDI backbone. The MTT experiment reveals that the cell viability of **47** treated cells is 110% at the concentration of 50 μg/mL, indicating **47** is noncytotoxic to living cells.

3. Biological applications of water-soluble perylenediimides

Water-soluble PDIs have been successfully applied in biological studies, because of their high fluorescence intensity and photostability, biocompatibility, and absorption and emission maxima above 500 nm to minimize the autofluorescence background of cells. Charged components are widely present in cells and tissues. For example, negatively charged extracellular matrixes support and connect the organization structure, and regulate the physiological activity of the organization and cell; negatively charged membranes provide a relatively stable internal environment for cell activities and regulate the cellular uptake and efflux of molecules. In addition, positively charged histone proteins and negatively charged DNA form DNA-protein complex for storing the genetic material. The ionic PDIs allow interactions with natural polyelectrolytes such as DNA or nuclear proteins through electrostatic interactions.

Non-ionic PEG, PG dendrons and dendritic carbohydrate derivatives have been widely used in biological studies. PEG is highly water soluble, biocompatible and nontoxic, and it shows no immunogenicity and possesses antifouling properties.

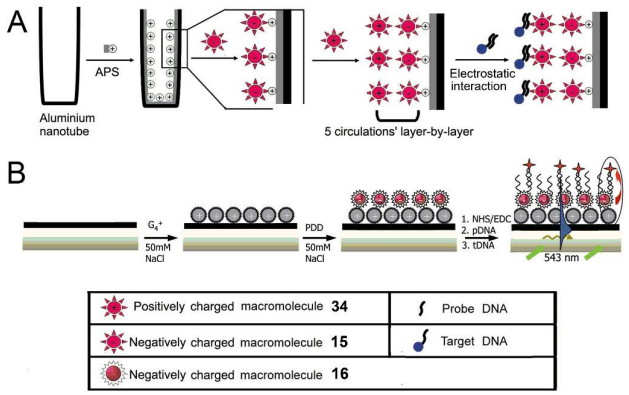

Fig. 17 A) Schematic diagram describing the formation of fluorescent nanotubes by layer-by-layer deposition of **15** and **34**. Reproduced with permission from ref. 27. Copyright 2011, John Wiley and Sons. B) Energy transfer between **16** donor and Cy5 acceptor. Reproduced with permission from ref. 51. Copyright 2011, John Wiley and Sons.

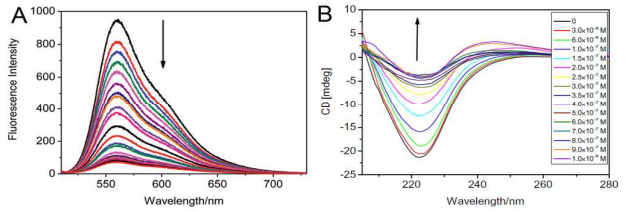

Fig. 18 A) Fluorescence spectra of **48** upon addition of Con A in PBS. Reproduced with permission from ref. 49. Copyright 2013, Royal Society of Chemistry. B) CD spectra of Con A in PBS upon addition of **49**. Reproduced with permission from ref. 48. Copyright 2013, Elsevier.

In addition, PEG can prolong the circulation time in the blood due to the resistance of nonspecific protein adhesion/denaturing. Therefore, it has been approved for medical use by the Food and Drug Administration (FDA). Hydrophilic PG dendrons show similar properties, such as highly biocompatible and minimal nonspecific interaction. Glycodendrimers exhibit the potential to recognize carbohydrate–protein (lectin) interactions involved in key biological processes, such as cell recognition, differentiation and adhesion.[48] The biological applications of water-soluble PDIs are summarized below from simple (basic) to complex (advanced) processes, including imaging studies of living cells, tissues and the whole body.

3.1 *In vitro* Studies

Due to the intrinsic fluorescence properties, the cationic or glycodendronized PDIs can be used as reporters for specific and sensitive detection of biological molecules. The interactions between functional PDIs and biomolecules provide the foundation for further studies in living cells, tissues and the whole body.

Fluorescent nanotubes fabricated by oppositely charged **34** and **15** were reported as DNA biosensors by Yin et al.[27] Positively charged **34** was deposited at surfaces and interacted with negatively charged DNA through electrostatic forces (Fig. 17A). Compared with the nanotube alone, the nanotube/DNA complex showed an increase in normalized fluorescence intensity because the hydrophilic DNA structures improved protection of the central PDI chromophore in the aqueous solution. Subsequently, Yin and coworkers developed a time-resolved, ultrasensitive and selective DNA sensor by combining fluorescence detection with energy transfer using the negatively charged **16** as donor molecule and Cy5 labeled DNA targets as acceptor molecule (Fig. 17B).[51] Upon excitation at 543 nm, excitation energy was transferred from the donor to the acceptor. Due to the high molar ratio of donor and acceptor, the fluorescence signal was greatly increased, achieving ultrasensitive and selective detection of DNA.

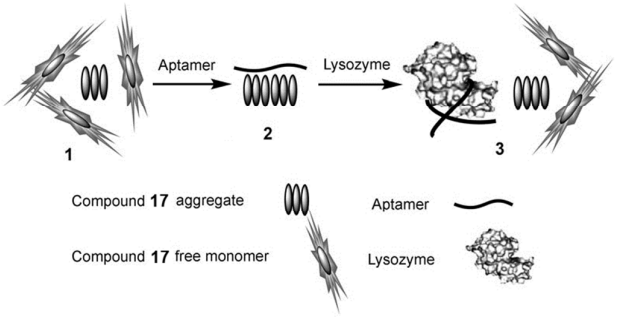

Fig. 19 Schematic diagram for selective detection of lysozyme. 1) Coexistence of the aggregates and monomer of **17** in aqueous solution; 2) binding of aptamer to **17** aggregates; 3) **17** is replaced by lysozyme, thus its monomer is released and the fluorescence is turn-on. Reproduced with permission from ref. 29. Copyright 2010, John Wiley and Sons.

PDI-cored glycodendrimers **48** and **49** showed selective binding to Concanavalin A (Con A) due to the carbohydrate–lectin interaction of the peripheral mannose moieties and Con A (a model lectin).[48, 49] Fluorescence spectroscopy and circular dichroism (CD) measurements were used to investigate the nature of the binding. As described in Fig. 18A, with increasing concentrations of Con A, the fluorescence emission of **48** exhibits a progressive decrease. The PDI backbones enter the hydrophobic region of Con A, via hydrogen bonds and hydrophobic interactions, leading to progressive quenching of fluorescence. Upon addition of **49**, the CD signal of the Con A, generated from the secondary-structure of β-sheet rich proteins, exhibits a progressive decrease and bathochromic shift (Fig. 18B). The loss of the secondary structure due to the formation of cross-linked complexes induces the decreased intensity of CD signal. The observed decrease of fluorescence emission intensity and CD signal intensity demonstrated the interactions of Con A with **48** or **49**.

A fluorescence turn-on approach for sensitive and selective detection of proteins based on nucleic acid aptamer and probe **17** is reported.[29] In aqueous solution, PDI **17** exists in both aggregated and monomeric forms, thus strong fluorescence can be detected. When negatively charged nucleic acid aptamer is added to the aqueous solution, PDI **17** rapid binds to the aptamer via the strong electrostatic interactions between the dye monomer/aggregates and the aptamer. When the monomer of **17** aggregates, a significant decrease in

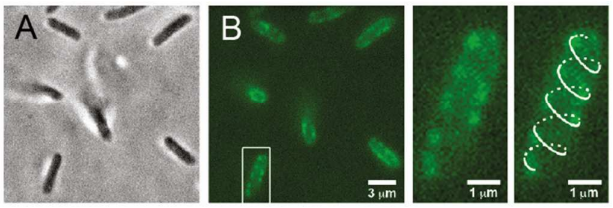

Fig. 20 A) Bright-field and B) fluorescence images of E. coli cells labeled with **46b**. Reproduced with permission from ref. 45. Copyright 2011, American Chemical Society.

the fluorescence intensity is observed. The lysozyme shows high affinity to aptamer. Upon the addition of lysozyme, **17** aggregates are replaced by the lysozyme. As a result, the monomer of **17** are released, and the fluorescence signal is turn-on (Fig. 19).

3.2 Live Cell Studies

Thanks to high selectivity and sensitivity, fluorescence bioimaging has been widely used in biological research because it offers a unique approach to visualize and manipulate the morphological details of cells and biological processes. Water soluble PDIs with high fluorescence intensity and biocompatibility have thus attracted great attention in bioimaging. Applications of water-soluble PDIs in live cell studies fall into three broad categories: the dye i) target-specifically labels receptors produced by bacteria, ii) is taken up into living cells via endocytic routes and accumulated in the cellular cytoplasm, plasma membrane, and small membrane-bound structures, or iii) carries DNA into the cell through electrostatic forces, which can be applied to gene delivery and bioimaging.

Zimmerman's group[45] reported a PG-dendronized PDI **46b** containing a single biotin used in target-specific fluorescent bioimaging. Biotinylated PDI **46b** could be immobilized on a PEG-passivated surface through biotin-neutravidin linkages with bright fluorescence, while only negligible binding of **46b** was observed without pre-incubated neutravidin, indicating that the immobilization was indeed highly specific. The target-specific fluorescent bioimaging was performed in living bacterial cells. *Escherichia coli* (E. coli) produced biotinylated λ receptors on the extracellular surface. The cells were pre-incubated with streptavidin. Fig. 20 shows that the bright fluorescent spots produced by **46b** appear only at the surfaces of the cells. Furthermore, the spots present a helical pattern along the long axis of the cell in some bacteria, which is consistent with the arrangement of the proteins on the bacteria surface. The above observation demonstrates that **46b** can be used as a highly target-specific label in bioimaging. This approach provides a new design for biolabeling by coupling a monofunctional fluorescent core to a multivalent periphery containing cellular receptors, therapeutic agents, targeting groups, or ligands.

A guanidinium-dendronized PDI **30** was reported for cellular cytoplasm imaging of HeLa cells (Fig. 21A).[35] The acquired images indicated that **30** was efficiently taken up into HeLa cells and accumulated in the cellular cytoplasm. Fluorescent, positively charged dendritic star polymers (**33**, **35** and **36**) were

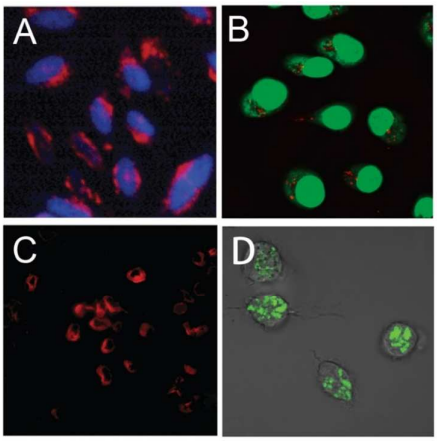

Fig. 21 A) Fluorescent microscopy images of HeLa cells stained with **30** (red) and cell nuclei stained with DAPI (blue). Reproduced with permission from ref. 35. Copyright 2013, Royal Society of Chemistry. B) Penetration of **33a** (red) into ECV-304 cells stained using a green fluorescence cell tracker. Reproduced with permission from ref. 25. Copyright 2008, American Chemical Society. C) Fluorescence images of HeLa cells stained with **39c**. Reproduced with permission from ref. 40. Copyright 2011, Royal Society of Chemistry. D) Confocal microscopic images of murine macrophage cells after incubation with **47**. Reproduced with permission from ref. 50. Copyright 2014, John Wiley and Sons.

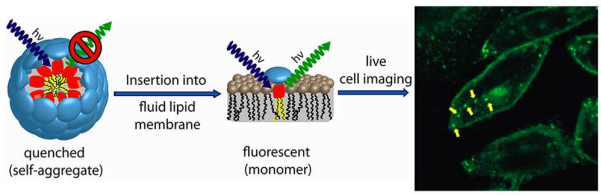

Fig. 22 Schematic diagram of the self-quenched amphiphilic dye **42** lighting up in fluid lipid membrane and confocal microscopy image of cells incubated with **42.** Reproduced with permission from ref. 44. Copyright 2013, American Chemical Society.

able to cross the cell membrane and enter living cells, whereas negatively charged dendritic star polymers (**14** and **16)** bearing carboxylic acids did not show any tendency to enter the cells.[25] For example, a confocal microscopy image of **33a** (red), which demonstrates penetration into the cells, is given in Fig. 21B. The authors reported that the PDIs bearing a higher density of polymer chains with fewer amino groups underwent faster cell entry; however, PDIs with high numbers of amino groups led to considerable cytotoxicity.

Besides the above cationic PDI, two non-ionic PDIs, **39c** and **47**, were also used for live-cell imaging.[40, 50] Fig. 21C reveals that **39c** is efficiently internalized by live-cells and accumulated in the cytoplasm. Based on the successful demonstration of binding interactions between **48** or **49** with Con A, the interaction was further investigated via confocal microscopy in macrophage cells. These cellular uptakes are mannose receptor-mediated and the cells possess selective binding with mannosylated derivatives. The green fluorescence of **47** inside the cell (Fig. 21D) suggested that the endocytosis mechanism led to vesicular (endosomal) localization. Control experiments indicated no obvious fluorescence by using another water-soluble PDI with cyclodextrin conjugates, suggesting that **47**

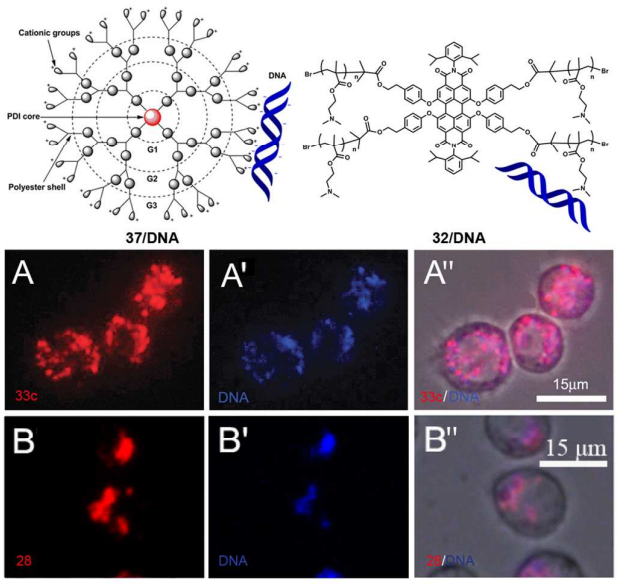

Fig. 23 Fluorescence images of the **37c**/DNA complex (A–A″) and **32**/DNA (B–B″) internalizing into cells after incubation. A and B are fluorescence images of **37c** and **32** (red), respectively. A′ and B′ are fluorescence images of CXR Reference Dye labeled DNA (blue). Reproduced with permission from ref. 38. Copyright 2013, Royal Society of Chemistry. Reproduced with permission from ref. 36. Copyright 2014, American Chemical Society.

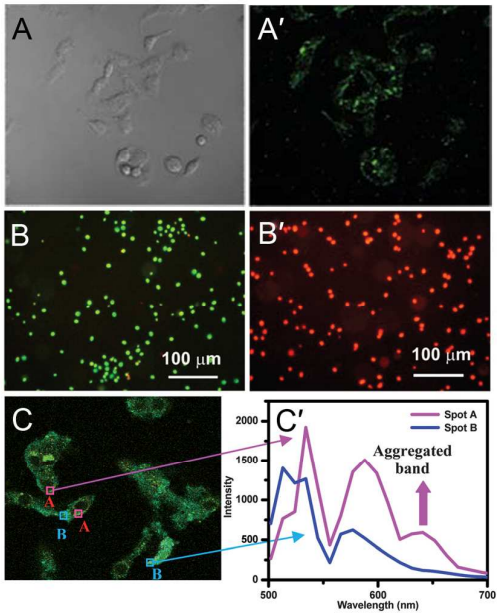

Fig. 24 A) Bright-field and A′) fluorescence images of HeLa cells after co-incubated with **40** and avidin. Reproduced with permission from ref. 41. Copyright 2013, Royal Society of Chemistry. Fluorescence images of the yeast suspensions for concentration of **26** B) 1×10^{-6} M and B′) 1×10^{-5} M. Reproduced with permission from ref. 33. Copyright 2013, Royal Society of Chemistry. C) Lambda scan image and C′) the corresponding emission intensity *vs.* wavelength plots. Reproduced with permission from ref. 19. Copyright 2012, Royal Society of Chemistry.

possessed selective binding interactions with the surface mannose receptor of the macrophage cells.

An amphiphilic PG-dendronized PDI **42** was reported as a membrane marker.[44] For highly specific membrane labeling, two alkyl chains were used as membrane anchoring groups and the length of the aliphatic chains was chosen to ensure the overall length of the hydrophobic part match the thickness of one lipid bilayer leaflet. In water, chromophore **42** formed micelleular aggregates and was nearly nonfluorescent. However, when **42** was incorporated into a lipophilic environment, such as inside biological membranes, the micelles disaggregated and the fluorescence of the perylene core was restored (Fig. 22). Cellular uptake studies documented that **42** was accumulated in the plasma membrane and in small vesicular structures such as Golgi, suggesting that it is taken up into living cells via endocytosis. Furthermore, the stained intracellular structures arose from a passive diffusion of **42** through the plasma membrane, as no colocalization of **42** and BODIPY TR methyl ester, which efficiently stains membranes of intracellular organelles, was shown with the exception of the Golgi. PG-dendronized PDI **42** is thus an ideal label to anchor and track PG bound bioactive compounds in cellular membranes.

PDI-cored cationic dendrimers **37** (**a**-**c**) and star polymers **31-32** were used for gene delivery and bioimaging by Yin and coworkers.[36, 38] By using fluorescence microscopy, the cellular uptake experiments demonstrated that all the cationic PDIs were internalized into cells. The cell viabilities of **37** (**a**-**c**) and **31-32** are all above 90%, indicating that the cationic PDIs exhibit low cytotoxicity. All the positively charged **37** (**a**-**c**), **31** and **32** could act as DNA carriers because of the electrostatic forces with negatively charged DNA. The fluorescence images of **37c**/DNA and **32**/DNA complexes internalized into cells upon incubation (Fig. 23) displayed that **37c** (A–A″) and **32** (B–B″) were able to deliver DNA into cells. The gene transfection efficacies of **37** (**a**-**c**) decrease in the following order: **37a**>**37b**>**37c**. This observation can be attributed to larger outer branches and more positive charges. The cationic dendrimers and star polymers are explored as a general tool for in vivo gene transfection.

Some water-soluble PDIs have unique self-assembly properties, which have been used in biology research. PDI **40** with a biotin ligand in the *bay*-region was used as "off-on" fluorescent probe for detecting and tracking of proteins, which was driven by assembly-disassembly behavior.[41] In aqueous solution, compound **40** self-assembles into nanostructures with complete quenching of fluorescence. After the addition of target protein, the self-assembled nanostructures are disassembled since the probes bind to the targeted protein, resulting in a strong fluorescence signal. In the presence of avidin, **40** can be internalized by living cells (Fig. 24A-A′). Under physiological conditions, **26** behaves as a fluorogenic probe in biological cells, yielding a dosage-dependent green or red fluorescence.[33] *Saccharomyces cerevisiae* yeast cells were incubated with two concentrations of **26** in PBS (1×10^{-6} M and 1×10^{-5} M). The fluorescence microscopy images of the two samples are clearly different. Green emitting can be detected in the yeast cells at the low concentration of **26** (1×10^{-6} M, Fig. 24B), while a red emission centered at about 630 nm was detected at the high concentration (1×10^{-5} M, Fig. 24B′).

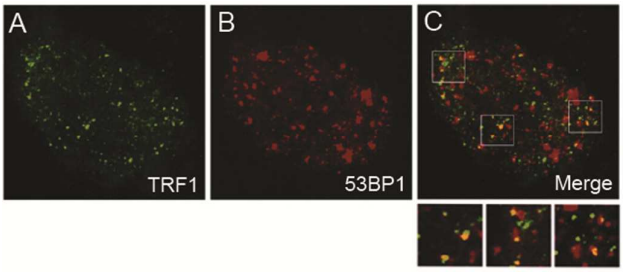

Fig. 25 Transformed (BJ-EHLT) human fibroblasts were treated with **19c**, fixed, and processed for IF by using antibodies against 53PB1. Representative images of IF by a Leica Deconvolution microscope. Enlarged views are below the merged images. Reproduced with permission from ref. 31. Copyright 2011, American Chemical Society.

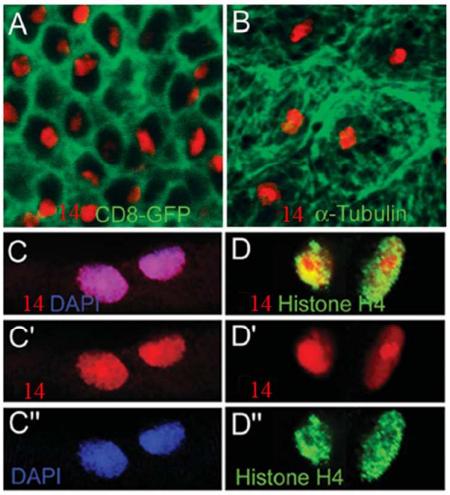

Fig. 26. Confocal images of *Drosophila* larval tissues stained by **14**. Double staining of **14** (red) with (A) CD8-GFP (green), (B) anti-α-Tubulin (green). (C-C") DAPI (blue), and (D-D") histone H4 (green). C', C" and D', D" are single channels. C and D are merged channels. Reproduced with permission from ref. 26. Copyright 2008, John Wiley and Sons.

Particularly, under strong visible light, the fluorescence of some specific cellular compartments can be turned from red to yellow and then to green, due to the photo-tuning process of **26**. The chiral PDI **7a** can be internalized by living cells, since the fluorescence is observed in the cytoplasm.[19] Taking advantage of the aggregation of **7a** *in vitro*, the pH of different regions of the cellular environment can be estimated. In the lambda scanning image (excitation wavelength = 488 nm, Fig 24C), co-existence of aggregated (640 nm) and monomeric emissions (550 nm and 590 nm) are observed in spot A, indicating that the pHs of these areas are below 4.5. In contrast, only monomeric emissions (580 nm) are observed in spot B, indicating the pH is above 4.5.

N-cyclic *bay*-substituted PDIs **19** (**a**-**j**) were reported as G-quadruplex ligands, causing DNA damage in transformed cells.[31] Modifications of the ending groups or the length of side chains at the *imide*-positions did not result in major changes of the affinity to the G-quadruplex formed by the human telomeric sequence. On the contrary, the number or the nature of the groups in the *bay*-region has a large influence on the affinity. Transformed human fibroblasts (BJ-EHLT) were

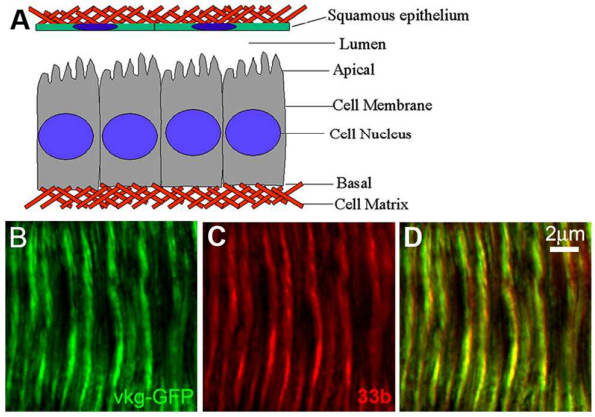

Fig. 27 Schematic illustration of extracellular matrix in a small central section of the Drosophila wing disc epithelium (A). Confocal images of ECM staining with **33b** (red, C), Vkg-GFP (green, B) in living tracheal epithelium and merged channels (D). Reproduced with permission from ref. 37. Copyright 2008, American Chemical Society.

incubated with **19c**. Deconvolution microscopy images revealed that some of the damaged foci containing phosphorylated 53BP1 (a DNA-damage response factor) were induced by **19c** co-localized with TRF1 (an effective interphase telomeres marker), forming the so-called telomere-dysfunction induced foci (TIFs) (Fig. 25). The G-quadruplex binding compound **19c** can act as a telomere inhibitor and exhibit the potential as a selective antineoplastic drug.

3.3 Tissue Imaging and Body Studies

Tissue imaging is usually achieved by fluorescence labeling, which is the process of covalently or non-covalently attaching a reactive derivative of the fluorophore to a functional group in the target molecule. The most commonly labeled objects are antibodies, proteins, amino acids, and peptides. Electrostatic interaction is very common in tissue imaging because there are many electrolytes in biological bodies.

Although the negatively charged dendritic star polymer **14** did not enter the cells,[25] it could specifically label the cell nucleus by binding to positively charged nuclear proteins and in fixed tissues.[26] Fixed *Drosophila* larval tissues were used to demonstrate the binding interaction of **14** and the nuclear proteins. As described in Fig. 26, **14** staining (red) shows no overlap with CD8-GFP (cell-membrane marker, green, Fig. 26A) or with anti-a-Tubulin antibodies (cytoskeletal marker, green, Fig. 26B). In Fig. 26C and 26D, **14** staining is in accordance with DAPI (DNA dye, blue, Fig. 26C") and demonstrates a significant co-localization with histone H4 (green, Fig. 26D"). Compound **14**, bearing multiple -COOH groups, was demonstrated to bind specifically and directly with positively charged histones, resulting in the labeling of the cell nucleus. The compound **14** offers an attractive alternative to conventional expensive antibodies or chromophores displaying broad emission spectra such as DAPI.

The positively charged dendritic star polymer **33b** was able to enter and label living cells.[25] In 2008, Yin et al[37] proposed a

new application of **33b** to directly stain the extracellular matrix (ECM) (Fig. 27A) network at high resolution and achieve (ECM)

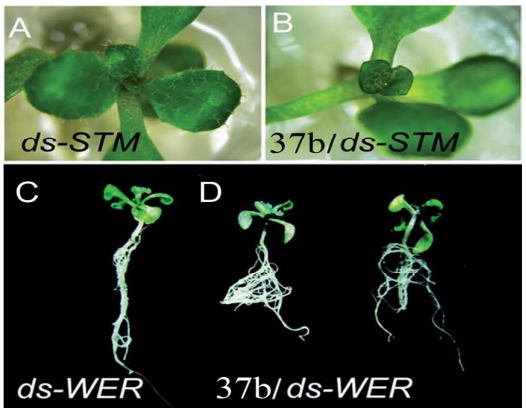

Fig. 28 Shoot morphological images of (A) H_2O/ds*STM*-treated (control) and (B) **37b**/ds*STM*-treated plants. Root morphology of (C) H_2O/ds*WER*-treated (control) and (D) **37b**/ds*WER*-treated roots. Reproduced with permission from ref. 52. Copyright 2014, Royal Society of Chemistry.

network visualization firstly. The positively charged chromophore **33b** was strongly bound to the negatively charged constituents of ECM in both fixed and living tissue via electrostatic forces. The confocal images of ECM staining with **33b** (red, Fig. 27C) and Vkg-GFP (green, Fig. 27B) in living trachea epithelium are presented in Fig. 27. By using high resolution confocal microscopy, **33b** staining almost completely overlapped with Vkg-GFP (Fig. 27D), indicating that **33b** gave the same specificity as Vkg-GFP for the ECM micronetwork structure. The ECM staining with **33b** was much faster than antibody staining procedures, which may require several days to complete. Spectral analysis reveals a significantly increased emission intensity of **33b** after binding to ECM components, supporting the direct binding between negatively charged ECM components and **33b**. All these observations support that **33b** is an efficient and specific ECM labeling agent.

In addition to the applications in the detection and imaging of biological molecules, some water-soluble PDIs can be used as gene/drug carriers or DNA intercalator together with simultaneous imaging in plants, insects and mice. Thus, these PDIs can be applied in the fields of diagnosis and therapy, which have attracted great attention in recent years. PDI-cored cationic dendrimers **37**(**a-c**) have been successfully applied to deliver DNA into animal cells *in vitro* by Yin and coworkers.[38]

Apart from the above application, the authors have applied **37b** as non-viral gene-vectors in plants using *Arabidopsis* as a model plant.[52] Fluorescence images displayed that **37b** was able to pass through the cell wall and deliver DNA efficiently throughout the root tissues, because **37b** and DNA were detected in both root cap and hair. The 10-day-old seedlings were treated with **37b**/dsRNA by dropping the complex solution to the seedling root. Two genes, *SHOOT MERISTEMLESS* (*STM*) and *WEREWOLF* (*WER*), which are essential for shoot tip and root development respectively, were chosen as target genes. **37b**/ds*STM*-treated plants exhibit smaller shoot tip compared with the control, which is

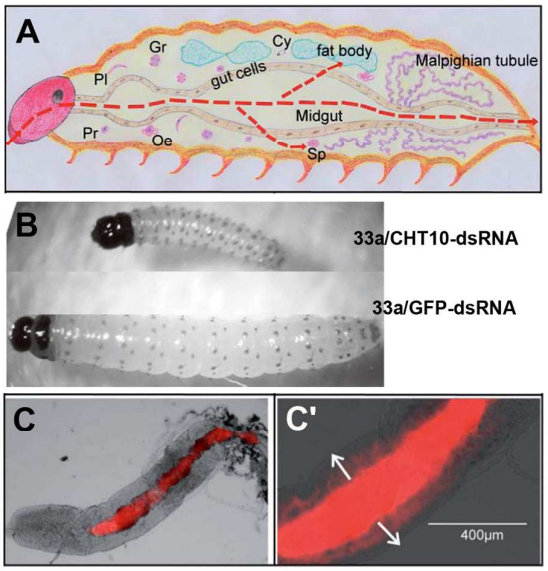

Fig. 29 A) Schematic diagram for longitudinal section of an insect larva. Reproduced with permission from ref. 54. Copyright 2014, Royal Society of Chemistry. B) Corn borer larvae fed with **33a**/CHT10-dsRNA and **33a**/GFP-dsRNA. Reproduced with permission from ref. 53. Copyright 2013, John Wiley and Sons. C) Fluorescence images of dissected larval gut after three days oral feeding of **37b**. C') part of enlarged C, red: **37b**. Reproduced with permission from ref. 54. Copyright 2014, Royal Society of Chemistry.

treated with H_2O/dsRNA (Fig. 28(A, B)). The root morphology after H_2O/ds*WER* and **37b**/ds*WER*-treatment are given in Fig. 28 (C, D). **37b**/ds*WER*-treated plants produced more lateral roots compared with the control. These observations reveal that **37b** can efficiently deliver dsRNA into plant cells and cause gene silencing with systemic phenotypes. The dendrimer **37b** provides a new platform for gene transfection and systemic gene silence of important developmental genes in plants.

Yin and coworkers[53] first reported that the cationic and PDI-cored dendritic star polymer **33a** was able to deliver dsRNA to kill insect pests in oral feeding experiments. To kill insect pests, such as the corn borer, CHT10-dsRNA was synthesized to silence a key developmental gene and GFP-dsRNA was used as control. Fig. 29A presents a schematic diagram of a longitudinal section of the insect with red lines indicating the spreading directions of the gene-vectors. As demonstrated in Fig. 29B, **33a**/CHT10-dsRNA fed larvae are clearly smaller than **33a**/GFP-dsRNA fed ones. Moreover, all the **33a** /CHT10-dsRNA-fed larvae died due to defective growth and molting. The *in vivo* experiments provided firm evidence that dsRNA was delivered into insect cells and efficiently silenced the target gene. Subsequently, the authors reported another gene vectors **37b**, which also exhibited high gene transfection and gene interference performance *in vivo* via oral feeding.[54] After three days of oral feeding, **37b** (red) is observed in the mid-gut and penetrated into the gut cells (Fig. 29C and C'). This non-viral gene delivery system opens a new avenue for the control

of insect pests without using chemical insecticides, which could cause environmental pollution.

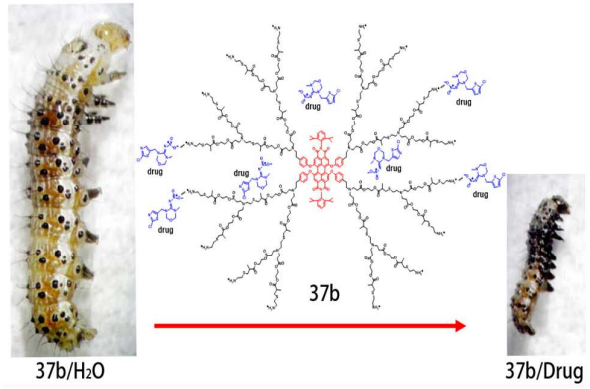

Fig. 30 The structure of **37b**/drug complexes and the digital photographs of larvae fed with diet containing **37b**/H_2O and **37b**/drug complexes. Reproduced with permission from ref. 55. Copyright 2014, Royal Society of Chemistry.

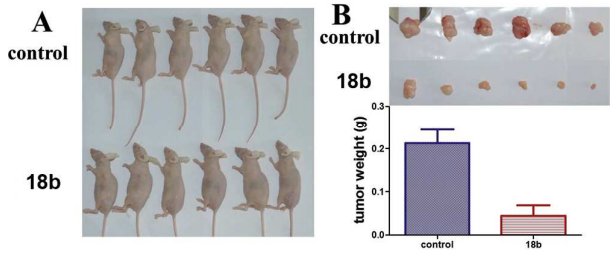

Fig. 31 Antitumor activity of PBDI was evaluated *in vivo*. A) Mice injected with **18b** (15 mg kg^{-1} per injection). In the control group, mice were injected with the same volume of stroke-physiological saline solution (SPSS). B) Tumor size and weight of dissected tumors from (A). Reproduced with permission from ref. 8. Copyright 2014, John Wiley and Sons.

Besides the above applications in gene delivery, **37b** was also used as hydrophobic drug carrier by Yin et al. due to the cavities provided by outer dendritic polyester units.[55] The dendrimer-based nanocarriers could efficiently deliver the drug into the live cells and largely increase the cytotoxicity of the drug. The larvae fed with **37b**/thiamethoxam complexes possess a smaller size than that of the controls fed with **37b**/H_2O (Fig. 30). Furthermore, after five day's feeding with **37b**/thiamethoxam complexes, more than 90% larvae died. The in *vivo* experiments indicate that the drug toxicity was greatly enhanced with the help of **37b**-mediated cellular internalization.

Yin and coworkers[8] reported a perylene-based DNA intercalator **18b** that could efficiently localize at the cell nucleus and inhibit cancer cell and tumor growth. The small cationic groups are incorporated in the *imide*-positions of PDIs to generate water solubility and maintain the planar structure of **18b**, which provides the potential for use as a DNA intercalator. Spectral analyses show that **18b** specifically accumulates in the cell nuclei by strong interaction with DNA. Chromophore **18b** shows a stronger suppression effect to cancer cells, which is attributed to the effective DNA intercalation and nuclear accumulation that leads to the inhibition of cancer cells. However, **18b** possesses a lower cytotoxicity to non-cancer cells, because of the much higher DNA replication rate of cancer cells than that of normal cells. Furthermore, with **18b** intercalation, DNA replication of cancer cells is inhibited more strongly than that of normal cells, which leads to the higher toxicity to cancer cells. Mice with HCT116 tumors were used as model to investigate the antitumor activity of **18b**. The body weights of the mice were not changed after 10 days of injection with **18b**. In addition, the tumor sizes are significantly smaller than those of the control (Fig. 31). The DNA intercalator **18b** with low toxicity is a potential anti-cancer drug for the suppression of cancer cells and tumors. Because of DNA intercalation, this type of PDIs could be developed as potential drugs for suppressing the cancer cells and tumors.

4. Conclusions and outlook

This review summarizes the design and synthesis of water-soluble PDIs as well as their biological applications. The synthetic strategies leading to water-soluble PDIs include the introduction of ionic or non-ionic substituents with multiple polar groups in the *bay*-region, *imide*- or *ortho*-positions of PDIs. The biological applications include simple to complex studies: *in vitro* studies, live cell studies, tissue and body imaging. Due to the fluorescent nature of the central PDI fluorophore, which allows for the tracing of cellular uptake via fluorescence microscopy, biological applications can be visualized using optical spectroscopy, energy transfer imaging, and other bioimaging techniques. Nevertheless, due to the undesirable self-aggregation, low FQY of PDI fluorophores in aqueous solution and low cytotoxic selectivity toward cancer cells, the synthesis of multi-functional water-soluble PDIs with useful applications in biological fields is still a topic of ongoing research. Despite of these challenges, a promising future of water-soluble PDIs can still be predicted. Look ahead, water-soluble PDIs with multiple functions will find wide applications such as simultaneous imaging with high specificity, diagnosis with high accuracy, and therapy with few side effects. The combination of fluorescence techniques and nanotechnology in biological applications will remain an active research area in the future, which can be supported by facile synthetic routes to multi-functional and water-soluble PDIs with high biological specificity.

Acknowledgements

This work was financially supported by the National Natural Science Foundation of China (21174012, 51221002 and 21574009), the Beijing Natural Science Foundation (2142026), the Innovation and Promotion Project of Beijing University of Chemical Technology, and the Fundamental Research Funds for the Central Universities (YS201402).

Notes and references

1. C. Huang, S. Barlow and S. R. Marder, *J. Org. Chem.*, 2011, **76**, 2386-2407.
2. J. Qu, J. Zhang, A. C. Grimsdale, K. Müllen, F. Jaiser, X. Yang and D. Neher, *Macromolecules*, 2004, **37**, 8297-8306.
3. L. Schmidt Mende, A. Fechtenkötter, K. Müllen, E. Moons, R. Friend and J. MacKenzie, *Science*, 2001, **293**, 1119-1122.
4. C. Li and H. Wonneberger, *Adv. Mater.*, 2012, **24**, 613-636.
5. H. Langhals, W. Jona, F. Einsiedl and S. Wohnlich, *Adv. Mater.*, 1998, **10**, 1022-1024.
6. D. Görl, X. Zhang and F. Würthner, *Angew. Chem. Int. Ed.*, 2012, **51**, 6328-6348.
7. K. Liu, Z. Xu, M. Yin, W. Yang, B. He, W. Wei and J. Shen, *J. Mater. Chem. B*, 2014, **2**, 2093-2096.
8. Z. Xu, K. Guo, J. Yu, H. Sun, J. Tang, J. Shen, K. Müllen, W. Yang and M. Yin, *Small*, 2014, **10**, 4087-4092.
9. C. Kohl, T. Weil, J. Qu and K. Müllen, *Chem. Eur. J.*, 2004, **10**, 5297-5310.
10. L. Zhong, F. Xing, W. Shi, L. Yan, L. Xie and S. Zhu, *ACS Appl. Mater. Interfaces*, 2013, **5**, 3401-3407.
11. K. Peneva, G. Mihov, F. Nolde, S. Rocha, J. i. Hotta, K. Braeckmans, J. Hofkens, H. Uji‐i, A. Herrmann and K. Müllen, *Angew. Chem. Int. Ed.*, 2008, **47**, 3372-3375.
12. G. Battagliarin, M. Davies, S. Mackowiak, C. Li and K. Müllen, *ChemPhysChem*, 2012, **13**, 923-926.
13. S. Nakazono, Y. Imazaki, H. Yoo, J. Yang, T. Sasamori, N. Tokitoh, T. Cedric, H. Kageyama, D. Kim and H. Shinokubo, *Chem. Eur. J.*, 2009, **15**, 7530-7533.
14. S. Nakazono, S. Easwaramoorthi, D. Kim, H. Shinokubo and A. Osuka, *Org. Lett.*, 2009, **11**, 5426-5429.
15. G. Battagliarin, C. Li, V. Enkelmann and K. Müllen, *Org. Lett.*, 2011, **13**, 3012-3015.
16. G. Battagliarin, Y. Zhao, C. Li and K. Müllen, *Org. Lett.*, 2011, **13**, 3399-3401.
17. J. Qu, C. Kohl, M. Pottek and K. Müllen, *Angew. Chem. Int. Ed.*, 2004, **43**, 1528-1531.
18. F. Yukruk, A. L. Dogan, H. Canpinar, D. Guc and E. U. Akkaya, *Org. Lett.*, 2005, **7**, 2885-2887.
19. P. K. Sukul, P. K. Singh, S. K. Maji and S. Malik, *J. Mater. Chem. B*, 2013, **1**, 153-156.
20. G. R. Newkome, K. K. Kotta and C. N. Moorefield, *J. Org. Chem.*, 2005, **70**, 4893-4896.
21. C. D. Schmidt, C. Böttcher and A. Hirsch, *Eur. J. Org. Chem.*, 2007, **2007**, 5497-5505.
22. C. D. Schmidt, C. Böttcher and A. Hirsch, *Eur. J. Org. Chem.*, 2009, **2009**, 5337-5349.
23. C. D. Schmidt, N. Lang, N. Jux and A. Hirsch, *Chem. Eur. J.*, 2011, **17**, 5289-5299.
24. F. Morgenroth, E. Reuther and K. Müllen, *Angew. Chem. Int. Ed. Engl.*, 1997, **36**, 631-634.
25. M. Yin, C. R. Kuhlmann, K. Sorokina, C. Li, G. Mihov, E. Pietrowski, K. Koynov, M. Klapper, H. J. Luhmann and T. Weil, *Biomacromolecules*, 2008, **9**, 1381-1389.
26. M. Yin, J. Shen, R. Gropeanu, G. O. Pflugfelder, T. Weil and K. Müllen, *Small*, 2008, **4**, 894-898.
27. M. Yin, C. Feng, J. Shen, Y. Yu, Z. Xu, W. Yang, W. Knoll and K. Müllen, *small*, 2011, **7**, 1629-1634.
28. S. You, Q. Cai, K. Müllen, W. Yang and M. Yin, *Chem. Commun.*, 2014, **50**, 823-825.
29. B. Wang and C. Yu, *Angew. Chem. Int. Ed.*, 2010, **49**, 1485-1488.
30. Z. Xu, W. Cheng, K. Guo, J. Yu, J. Shen, J. Tang, W. Yang and M. Yin, *ACS Appl. Mater. Interfaces*, 2015, **7**, 9784-9791.
31. V. Casagrande, E. Salvati, A. Alvino, A. Bianco, A. Ciammaichella, C. D'Angelo, L. Ginnari-Satriani, A. M. Serrilli, S. Iachettini, C. Leonetti, S. Neidle, G. Ortaggi, M. Porru, A. Rizzo, M. Franceschin and A. Biroccio, *J. Med. Chem.*, 2011, **54**, 1140-1156.
32. M. Lor, J. Thielemans, L. Viaene, M. Cotlet, J. Hofkens, T. Weil, C. Hampel, K. Müllen, J. W. Verhoeven and M. Van der Auweraer, *J. Am. Chem. Soc.*, 2002, **124**, 9918-9925.
33. M. Montalti, G. Battistelli, A. Cantelli and D. Genovese, *Chem. Commun.*, 2014, **50**, 5326-5329.
34. J. Schönamsgruber, B. Schade, R. Kirschbaum, J. Li, W. Bauer, C. Böttcher, T. Drewello and A. Hirsch, *Eur. J. Org. Chem.*, 2012, **2012**, 6179-6186.
35. J. Zhou, J. Zhang, Y. Lai, Z. Zhou, Y. Zhao, H. Wang and Z. Wang, *New J. Chem.*, 2013, **37**, 2983-2986.
36. S. You, Q. Cai, Y. Zheng, B. He, J. Shen, W. Yang and M. Yin, *ACS Appl. Mater. Interfaces*, 2014, **6**, 16327-16334.
37. M. Yin, J. Shen, G. O. Pflugfelder and K. Müllen, *J. Am. Chem. Soc.*, 2008, **130**, 7806-7807.
38. Z. Xu, B. He, J. Shen, W. Yang and M. Yin, *Chem. Commun.*, 2013, **49**, 3646-3648.
39. Z. Xu, B. He, W. Wei, K. Liu, M. Yin, W. Yang and J. Shen, *J. Mater. Chem. B*, 2014, **2**, 3079-3086.
40. B. Gao, H. Li, H. Liu, L. Zhang, Q. Bai and X. Ba, *Chem. Commun.*, 2011, **47**, 3894-3896.
41. F. Bo, B. Gao, W. Duan, H. Li, H. Liu and Q. Bai, *RSC Adv.*, 2013, **3**, 17007-17010.
42. T. Heek, C. Fasting, C. Rest, X. Zhang, F. Würthner and R. Haag, *Chem. Commun.*, 2010, **46**, 1884-1886.
43. T. Heek, F. Würthner and R. Haag, *Chem. Eur. J.*, 2013, **19**, 10911-10921.
44. T. Heek, J. r. Nikolaus, R. Schwarzer, C. Fasting, P. Welker, K. Licha, A. Herrmann and R. Haag, *Bioconjug. Chem.*, 2013, **24**, 153-158.
45. S. K. Yang, X. Shi, S. Park, S. Doganay, T. Ha and S. C. Zimmerman, *J. Am. Chem. Soc.*, 2011, **133**, 9964-9967.
46. S. K. Yang and S. C. Zimmerman, *Adv. Funct. Mater.*, 2012, **22**, 3023-3028.
47. A. T. Zill, K. Licha, R. Haag and S. C. Zimmerman, *New J. Chem.*, 2012, **36**, 419-427.
48. K. Wang, Y. Wang, J. Li, H. An, L. Zhang, J. Zhang and X. Li, *Bioorg. Med. Chem. Lett.*, 2013, **23**, 480-483.
49. K. Wang, H. An, F. Qian, Y. Wang, J. Zhang and X. Li, *RSC Adv.*, 2013, **3**, 23190-23196.
50. K. Wang, H. An, R. Rong, Z. Cao and X. Li, *Macromol. Rapid Commun.*, 2014, **35**, 727-734.
51. C. L. Feng, M. Yin, D. Zhang, S. Zhu, A. M. Caminade, J. P. Majoral and K. Müllen, *Macromol. Rapid Commun.*, 2011, **32**, 679-683.

52. L. Jiang, L. Ding, B. He, J. Shen, Z. Xu, M. Yin and X. Zhang, *Nanoscale*, 2014, **6**, 9965-9969.
53. B. He, Y. Chu, M. Yin, K. Müllen, C. An and J. Shen, *Adv. Mater.*, 2013, **25**, 4580-4584.
54. D. Shen, F. Zhou, Z. Xu, B. He, M. Li, J. Shen, M. Yin and C. An, *J. Mater. Chem. B*, 2014, **2**, 4653-4659.
55. X. Liu, B. He, Z. Xu, M. Yin, W. Yang, H. Zhang, J. Cao and J. Shen, *Nanoscale*, 2015, **7**, 445-449.